INTERNATIONAL JOURNAL OF NUMERICAL METHODS IN FLUIDS, VOL. 13, 537–556 (1991)

THREE-DIMENSIONAL LAMINAR FLOW AND HEAT TRANSFER IN THE ENTRANCE REGION OF TRAPEZOIDAL DUCTS

BIJAN FARHANIEH AND BENGT SUNDEN

Department of Applied Thermodynamics and Fluid Mechanics, Chalmers University of Technology, S-41296 Göteborg, Sweden

SUMMARY

The laminar convective flow and heat transfer in a duct with a trapezoidal cross-sectional area are studied numerically. The governing equations are solved numerically by a finite volume formulation in complex three-dimensional geometries using co-located variables and Cartesian velocity components. Details of the numerical method are presented. The accuracy of the method was also established by comparing the calculated results with the analytical and numerical results available in the open literature. The Nusselt numbers are obtained for the boundary condition of a uniform wall temperature whereas the friction factors are calculated for no-slip conditions at the walls. The asymptotic values of the Nusselt numbers, friction factors. incremental pressure drops, axial velocity and momentum rate and kinetic energy correction factors approach the available fully developed values. Various geometrical dimensions of the cross-section are considered.

KEY WORDS Three-dimensional Flow and heat transfer Trapezoidal duct Entrance region

INTRODUCTION

Ducts with trapezoidal shapes are commonly used in regenerative heat exchanges. Such heat exchangers are employed in thermal power plants as preheaters and in air-conditioning systems as heat recovery units. The fluid flow in the ducts is three-dimensional, and owing to the small hydraulic diameter of the duct, the Reynolds number becomes so small that laminar flow may prevail along the duct.

Several studies of laminar and laminar fully developed flow in ducts with various cross-sections have been presented in the past. Patankar and Spalding[1] developed a calculation procedure in 1972 for three-dimensional parabolic flows. This methodology was later used by Prakash and Lui[2] to study the forced convective flow and heat transfer in the entrance region of an internally finned circular duct. Karki and Patankar[3] adopted this method in their studies of buoyancy effects in the entrance region of a shrouded fin array. In 1974 Shah[4] adopted a least-squares matching technique to analyse fully developed laminar flow and heat transfer in ducts of arbitrary cross-sections. Shah and London[5] in 1978 gathered a summary of the literature on heat transfer in laminar duct flow in a book. Baliga and Azrak,[6] Kays and London,[7] Schmidt and Newell,[8] Sparrow and Haji-Sheikh[9] and Schneider and LeDain[10] are a few more who have investigated three-dimensional laminar fully developed flow and heat transfer in ducts of triangular cross-

0271–2091/91/150537–20$10.00

Received September 1990

section. Faghri *et al.*[11] in 1984 developed a numerical method which utilizes an algebraic co-ordinate transformation to map an irregular cross-section onto a rectangular one and adopts the calculation procedure for three-dimensional parabolic problems developed by Patankar *et al.*[1] This method was used to investigate the three-dimensional laminar heat transfer and fluid flow characteristics in the entrance region of a regular polygonal duct[12] and a rhombic duct.[13] Zhang *et al.*[14] obtained hydrodynamically fully developed flow and developing temperature field in ducts with triangular and semicircular cross-sections.

A literature survey of the available works points out the lack of thorough studies of three-dimensional laminar flow and heat transfer characteristics in the hydrodynamic and thermal entrance regions of trapezoidal ducts.

The numerical method used in the present work is a finite volume method for elliptic flows in complex three-dimensional geometries which utilizes co-located variables and Cartesian velocity components. In this paper the method is applied to laminar forced convective flow and heat transfer in trapezoidal ducts.

Numerical solutions were carried out for a uniform wall temperature at four values of the duct angle ϕ and three values of the aspect ratio α.

PROBLEM FORMULATION

The trapezoidal duct to be studied is presented schematically in Figure 1. A symmetry surface divides the duct into two identical channels. Advantage is taken of this feature to limit the calculation domain to only half of the total cross-sectional area. The heat transfer and fluid flow characteristics for laminar, incompressible, forced convection in the entrance region are to be determined. The inlet conditions (uniform velocity and temperature) are also presented in the figure. The walls of the duct are kept at a uniform temperature. The axial velocity is in the x-direction.

The governing equations are the continuity, momentum and energy equations. Consideration is given to simultaneously developing laminar flow. The flow is studied under the following assumptions: steady state, constant fluid properties, negligible viscous dissipation and no natural convection. The following dimensionless variables are introduced:

$$X_i=\frac{x_i}{D_h}, \qquad U_i=\frac{u_i}{u_{in}}, \qquad P=\frac{p}{\rho u_{in}^2}, \qquad \Theta=\frac{T-T_{in}}{T_w-T_{in}}.$$

The governing equations now take the following forms in a Cartesian co-ordinate system:

$$\frac{\partial U_i}{\partial X_i}=0, \tag{1}$$

$$U_j\frac{\partial \Psi}{\partial X_j}=\Gamma\frac{\partial^2 \Psi}{\partial X_j \partial X_j}+S_\Psi, \tag{2}$$

where Γ is equal to $1/Re$ in the momentum equations and to $1/RePr$ in the energy equation. The source term S_Ψ is equal to $\partial P/\partial X_i$ in the momentum equations and to zero in the energy equation. The boundary conditions at the inlet of the duct are

$$V=W=0, \qquad U=1 \quad \text{(uniform)}, \qquad \Theta=0 \quad \text{(uniform)}.$$

At the walls we have

$$U_i=0, \qquad \Theta=1 \quad \text{(uniform)}.$$

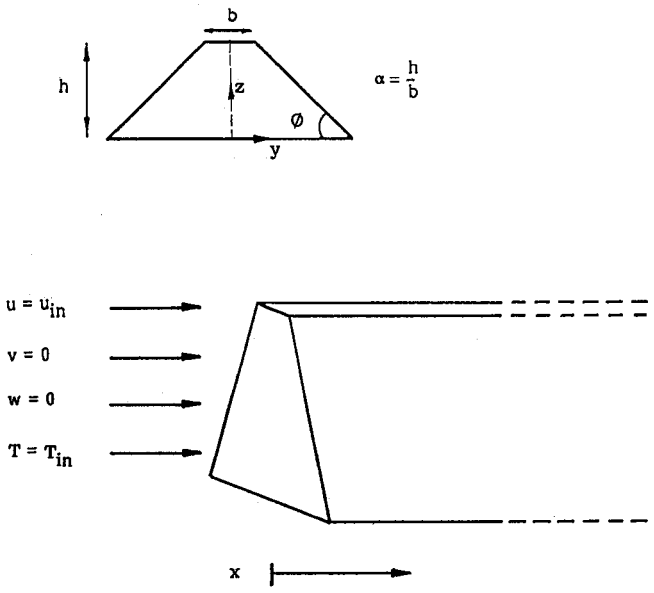

Figure 1. Trapezoidal duct

FLUID FLOW QUANTITIES

Pressure drop

The cross-sectional average pressure at any yz-plane is obtained by

$$\bar{P}=\frac{\sum_1^N P_i \delta A_i}{A}, \tag{3}$$

where δA_i is the area of the control volume face and A is the cross-sectional area.

The local friction factor f at any cross-section is defined as[5]

$$f=\frac{(-\mathrm{d}\bar{p}/\mathrm{d}x)\,D_\mathrm{h}/4}{\rho u_\mathrm{in}^2/2}. \tag{4}$$

In the fully developed region the local friction factor is inversely proportional to Re and $(fRe)_\mathrm{fd}$ is independent of x. The pressure drop in this region is caused only by the wall shear, whereas in the region of developing flow the pressure drop results from the wall shear as well as the change in momentum flow rate as the velocity profile develops. This latter contribution to the pressure drop is designated as the dimensionless incremental pressure drop number $K(x)$ and is defined by

$$K(x)=\frac{\Delta p}{\rho u_\mathrm{m}^2/2}-(fRe)_\mathrm{fd}\frac{4x}{D_\mathrm{h}Re}. \tag{5}$$

The second term on the right-hand side of the above equation represents the pressure drop if the flow is fully developed immediately downstream of the inlet.

In heat exchanger ducts the length of the ducts is usually several times the hydraulic diameter. Thus the ducts can be regarded as 'long ducts'. Therefore the knowledge of fully developed values of the friction factor f_fd and $K(\infty)$ is sufficient to establish the total pressure drop. Lundgren *et al.*

(see Reference 5) worked out an approximate analytical method to determine the incremental pressure drop in the fully developed region for ducts of arbitrary cross-section. The formula is

$$K(\infty)=\frac{2}{A}\int_A\left[\left(\frac{u_{fd}}{u_{in}}\right)^3-\left(\frac{u_{fd}}{u_{in}}\right)^2\right]dA. \tag{6}$$

Momentum rate

The momentum rate in the main flow direction at any cross-sectional plane along the duct is obtained by[4,5]

$$\text{MoR}=K_d(x)\rho u_{in}^2 A, \tag{7}$$

where $K_d(x)$ is the momentum flux correction factor and is defined by

$$K_d(x)=\frac{1}{A}\int_A\left(\frac{u}{u_m}\right)^2 dA. \tag{8}$$

Kinetic energy

The kinetic energy of the fluid in the main flow direction at any cross-sectional plane along the duct is calculated by[4,5]

$$\text{KE}=K_e(x)\frac{\rho u_{in}^3}{2}A, \tag{9}$$

where $K_e(x)$ is the kinetic energy correction factor and is defined by

$$K_e(x)=\frac{1}{A}\int_A\left(\frac{u}{u_m}\right)^3 dA. \tag{10}$$

The fully developed value of the incremental pressure drop may also be written in the following form by considering equations (6), (8) and (10):

$$K(\infty)=2[K_e(\infty)-K_d(\infty)]. \tag{11}$$

$K(\infty)$ determined by the above equation is generally higher than that measured experimentally[5] and might also deviate from the value obtained using the exact method presented in equation (5).

HEAT TRANSFER

The heat transfer results are expressed in terms of the dimensionless Nusselt number.

The local peripheral average Nu for non-circular ducts and the average Nu up to the axial location x are defined as

$$Nu_x=\frac{h_x D_h}{k}=\frac{D_h[(\partial T/\partial\eta)_{w,m}]_x}{T_w-T_b}, \tag{12}$$

$$Nu_m=\frac{h_m D_h}{k}=\frac{1}{x}\int_0^x Nu_x dx, \tag{13}$$

where $(\partial T/\partial\eta)_{w,m}$ represents the peripheral average temperature gradient at the wall. In equations (12) and (13) k is the thermal conductivity. The bulk temperature T_b at any axial location x is defined as

$$T_b=\frac{1}{Au_m}\int_A uT dA. \tag{14}$$

SOLUTION METHODOLOGY

In order to extend the capabilities of the finite difference method to deal with complex geometries, a boundary-fitted co-ordinate method is used.

The basic idea in this method is to map the complex flow domain in the physical space to a simple rectangular domain in the computational space by using a curvilinear co-ordinate transformation. In other words, the Cartesian co-ordinate system x_i in the physical domain is replaced by a general non-orthogonal system ξ_i.

The momentum equations are solved for the velocity components U, V, W in the fixed Cartesian directions on a non-staggered grid. This means that all the variables are stored at the centre of the control volume. This method was suggested and worked out by Rhie and Chow[15] and later used by Burns and Wilkes,[16] Majumdar,[17] Peric *et al.*[18] and Miller and Schmidt.[19] Majumdar[20] later discussed the importance of underrelaxation in momentum interpolation when non-staggered grids are used.

The steady transport equation for a general dependent variable Ψ in Cartesian co-ordinates can be written as

$$\frac{\partial}{\partial X_i}(\rho U_i \Psi) = \frac{\partial}{\partial X_i}\left(\Gamma \frac{\partial \Psi}{\partial X_i}\right) + S, \tag{15}$$

where Γ is the exchange coefficient and is constant in this case. The total flux (convective and diffusive fluxes) is defined as

$$I_i = \rho U_i \Psi - \Gamma \frac{\partial \Psi}{\partial X_i}. \tag{16}$$

It is now convenient to write equation (15) in the equivalent form

$$\frac{\partial I_i}{\partial X_i} = S \quad \text{or} \quad \nabla \mathbf{I} = S. \tag{17}$$

Integration of equation (17) over any control volume in the physical space, using Gauss's law, gives

$$\int_A \mathbf{I} \cdot \mathrm{d}\mathbf{A} = \int_V S \mathrm{d}V. \tag{18}$$

Equations (16) and (17) are used for performing the transformation to the computational space co-ordinates (general non-orthogonal co-ordinates) ξ_i.

The scalar advection–diffusion equation (18) is discretized. The integration of this gives

$$(\mathbf{I} \cdot \mathbf{A})_e + (\mathbf{I} \cdot \mathbf{A})_w + (\mathbf{I} \cdot \mathbf{A})_n + (\mathbf{I} \cdot \mathbf{A})_s + (\mathbf{I} \cdot \mathbf{A})_h + (\mathbf{I} \cdot \mathbf{A})_l = S \delta V, \tag{19}$$

where e, w, n, s, h and l refer to the faces of the control volume; see Figure 2. The discretized equation is rearranged in the standard form

$$a_P \Psi_P = \sum a_{NB} \Psi_{NB} + S_C, \tag{20}$$

where

$$a_P = \sum a_{NB} - S_P. \tag{21}$$

The coefficients a_{NB} contain the contributions due to convection and diffusion and the source terms S_P and S_C contain the remaining terms.

Convection

For the sake of conciseness and simplicity we restrict ourself in this and the following subsections only to the east face of the control volume for explanation of the numerical procedure. The total flux I contains convective and diffusive fluxes. The first term on the right-hand side of equation (16) is the convective term. The mass flow rate through the east face can be expressed as the scalar product of the velocity and area vectors multiplied by the density. Thus we have

$$\dot{m}_e = \rho_e \mathbf{u} \cdot \mathbf{A} = \rho_e (u_e A_{ex} + v_e A_{ey} + w_e A_{ez}), \tag{22}$$

where the Cartesian areas are calculated by

$$A_{ex} = |\mathbf{A}|_e \mathbf{n} \cdot \mathbf{e}_x, \qquad A_{ey} = |\mathbf{A}|_e \mathbf{n} \cdot \mathbf{e}_y, \qquad A_{ez} = |\mathbf{A}|_e \mathbf{n} \cdot \mathbf{e}_z. \tag{23}$$

Here $|\mathbf{A}|_e$ is the total area of the east face, $\mathbf{n}$ is its normal vector and $\mathbf{e}$ are the Cartesian base vectors. In order to obtain the velocity components on the control volume faces from those on the control volume centres, the Rhie–Chow[15] interpolation method is used. In this method the weighted linear interpolation in physical space, $u_e = f_x u_E + (1 - f_x) u_P$, is not used in order to avoid non-physical oscillations in pressure and velocity. The method can be described as follows. Consider the interpolation to the east face of a control volume centred at P; see Figure 3(a). The pressure gradient is subtracted from the velocity components stored at the centre of the control volumes:

$$u_P^o = u_P - \frac{-(P_e - P_w)\delta V}{|\overrightarrow{we}|(a_P)_P}, \qquad u_E^o = u_E - \frac{-(P_{ee} - P_e)\delta V}{|\overrightarrow{e(ee)}|(a_P)_E}. \tag{24}$$

The velocity component on the east face is now calculated as

$$u_e = f_x u_E^o + (1 - f_x) u_P^o + \text{pressure gradient},$$

$$u_e = f_x u_E^o + (1 - f_x) u_P^o - \frac{(P_E - P_P)\delta V}{|\overrightarrow{PE}|(a_P)_e}, \tag{25}$$

where f_x is the interpolation factor and is calculated by

$$f_x = \frac{|\overrightarrow{Pe}|}{|\overrightarrow{Pe}| + |\overrightarrow{eE}|}.$$

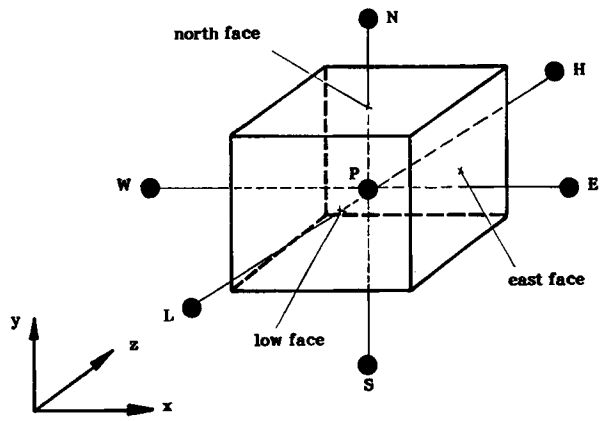

Figure 2. A control volume

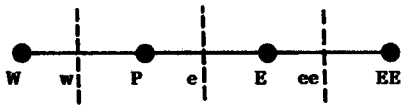

Figure 3(a). Grid nomenclature

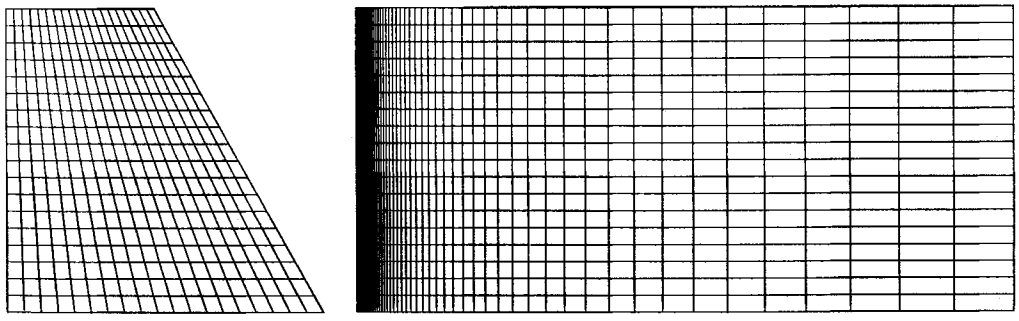

Figure 3(b). A typical grid presentation

P_e, P_w and P_{ee} in equation (24) are calculated by linear interpolation. As seen from equation (25), the pressure gradient is now calculated using the adjacent nodes of the east face. This avoids any non-physical oscillations in the pressure field. v_e and w_e are calculated in a similar manner.

Diffusion

The second term in the total flux $\mathbf{I}_i$ presented in equation (16) is the diffusion term. Through an area $\mathbf{A}$ we have

$$(\mathbf{I}\cdot\mathbf{A})_{\text{diff}} = -\Gamma\mathbf{A}\cdot\nabla\Psi. \tag{26}$$

$\mathbf{A}\cdot\nabla\Psi$ in equation (26) can for the east face be rewritten in Cartesian coordinates as

$$-(\mathbf{A}\cdot\nabla\Psi)_e = -\left(A_{ex}\frac{\partial\Psi}{\partial x}+A_{ey}\frac{\partial\Psi}{\partial y}+A_{ez}\frac{\partial\Psi}{\partial z}\right) \tag{27}$$

and in general non-orthogonal co-ordinates as

$$-(\mathbf{A}\cdot\nabla\Psi)_e = -\left(\mathbf{A}\cdot\mathbf{g}_i g^{ij}\frac{\partial\Psi}{\partial\xi_j}\right)_e = \left(|\mathbf{A}|\mathbf{n}\cdot\mathbf{g}_i g^{ij}\frac{\partial\Psi}{\partial\xi_j}\right)_e, \tag{28}$$

where $\mathbf{g}_i$ is the covariant base vector. The appearance of the metric tensor g^{ij} in equation (28) is due to the fact that the components of the product $\mathbf{A}\cdot\mathbf{g}_i$ and the derivative $\partial\Psi/\partial\xi_j$ are both covariant and the product of their contravariant base vectors is not zero for $i\neq j$ since they are non-orthogonal to each other.[20] The components of g^{ij} can be calculated as shown in Reference 21 for example.

The normal vector $\mathbf{n}$ in equation (28) is equal to the cross-product of $\mathbf{g}_2$ and $\mathbf{g}_3$, which implies that $\mathbf{n}\cdot\mathbf{g}_2\equiv\mathbf{n}\cdot\mathbf{g}_3\equiv 0$. Equation (28) can now be written as

$$-(\mathbf{A}\cdot\nabla\Psi)_e = \left(|\mathbf{A}|\mathbf{n}\cdot\mathbf{g}_1 g^{1j}\frac{\partial\Psi}{\partial\xi_j}\right)_e \quad \text{for} \quad j=1,\,2,\,3. \tag{29}$$

Pressure correction equation

The pressure correction equation is obtained by applying the SIMPLEC algorithm[22] on the non-staggered grid. The mass flux $\dot{m}$ is divided into one old value, $\dot{m}^*$, and another correction value, $\dot{m}'$. The mass flux correction at the east face can be calculated by

$$\dot{m}'_e = \rho \mathbf{A} \cdot \mathbf{u}' = \rho_e (A_{ex} u'_e + A_{ey} v'_e + A_{ez} w'_e) = (\rho A \cdot \mathbf{g}^j u'_j)_e, \tag{30}$$

where u'_j is the covariant correction velocity. The covariant velocity components are related to the pressure gradient by[23]

$$u_j = -\frac{1}{a_P} \frac{\partial p}{\partial x_j}. \tag{31}$$

By introducing equation (31) into equation (30), we obtain

$$\dot{m}'_e = \left[\rho \mathbf{A} \cdot \left(-\frac{1}{a_P} \frac{\partial p'}{\partial x_j} \mathbf{g}^j \right) \right]_e = -\left(\frac{\rho}{a_P} \mathbf{A} \cdot \nabla p' \right)_e. \tag{32}$$

Consider for simplicity the continuity equation in one dimension:

$$\dot{m} = \dot{m}_e - \dot{m}_w = 0. \tag{33}$$

If $\dot{m} = \dot{m}^* + \dot{m}'$ and equation (32) are substituted into equation (33), we obtain

$$\left(\frac{\rho}{a_P} \mathbf{A} \cdot \nabla p' \right)_w - \left(\frac{\rho}{a_P} \mathbf{A} \cdot \nabla p' \right)_e + \dot{m}^*_e - \dot{m}^*_w = 0. \tag{34}$$

This is a diffusion equation for the pressure correction p'. $\mathbf{A} \cdot \nabla p'$ can be calculated with equation (29) by replacing Ψ by p'.

COMPUTATIONAL DETAILS

The solution methodology presented in the preceding section was transferred to a computer code called CALC-BFC. It was originally developed by Davidson[23] but has been further developed in this work. The general structure of the code is similar to that of TEACHT and the equations are solved by a TDMA routine.

Grid

In order to investigate the grid size effect, computations were performed for $\phi = 45°$ and three different aspect ratios α under various grid sizes. Comparison of the $(fRe)_{fd}$ of each test and the values of Shah[4] are presented in Table I. To maintain relatively moderate computing costs in the final calculations, a 20×21 grid was used for $\alpha = 0{\cdot}5$ and 1 and a 25×25 grid was chosen for $\alpha = 2$. In the main flow direction a non-uniform grid with 82 step sizes generated by a power law formula with higher concentration close to the inlet of the duct was employed. Each control volume contains one node at its centre, whereas the boundary adjacent volumes contain two nodes. A typical grid is shown in Figure 3(b).

RESULTS AND DISCUSSION

Hydrodynamic results

Comparison with previous results. In Figure 4 the axial pressure distribution for $\phi = 90°$, $\alpha = 1$ is compared with the experimental data of Beavers *et al.*[24] The computed results are in reasonable

Table I. Grid size effect on $(fRe)_{fd}$ ($\phi = 45°$)

	$(fRe)_{fd}$		
Grid points	$\alpha = 0{\cdot}5$	$\alpha = 1$	$\alpha = 2$
12×12	14·825	13·260	12·709
15×15	14·983	13·424	13·041
20×21	15·052	13·594	13·212
25×25	15·145	13·782	13·234
30×30	—	—	13·307
Shah[4]	15·206	13·827	13·364

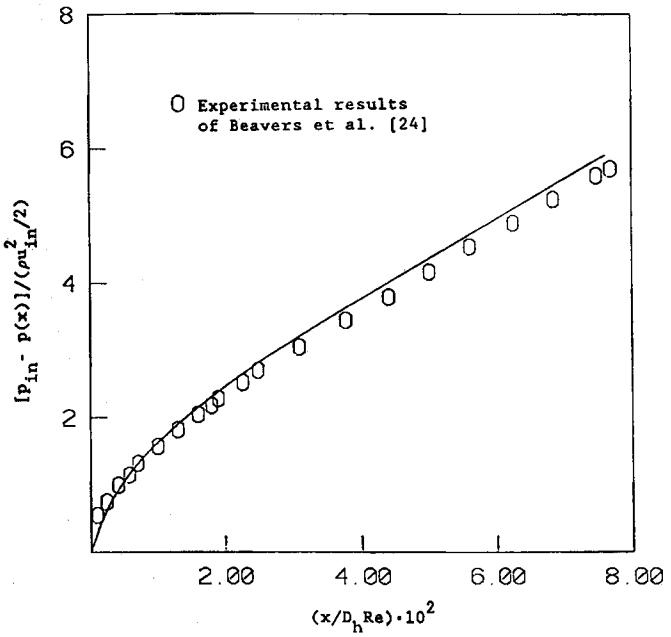

Figure 4. Comparison of the computed pressure drop with experimental data ($\phi = 90°$, $\alpha = 1$)

agreement with the experimental data. The (fRe)-values in the fully developed region agree well with the analytical values obtained by Shah.[4]

Incremental pressure drop. The incremental pressure drop $K(x)$ for different ϕ and aspect ratios is plotted in Figure 5. K increases with the axial distance x and approaches asymptotically a constant value in the fully developed region as can be seen in Figure 5. $K(\infty)$ represents the total incremental pressure drop due to the entrance effect and can be calculated either graphically by extrapolating the results in Figure 5 or by using equation (11); see Table II. The values of $K(\infty)$ obtained by these two methods are not in exact agreement with each other. This can be due to the fact that the method presented in equation (11) is an approximate method but also due to an insufficient number of grid points.

Axial velocity vectors and contours. The velocity vectors of the cross-stream flow (secondary flow) for $\phi = 60°$, $\alpha = 1$ are presented in Figure 6 at three different axial positions. As is evident, the

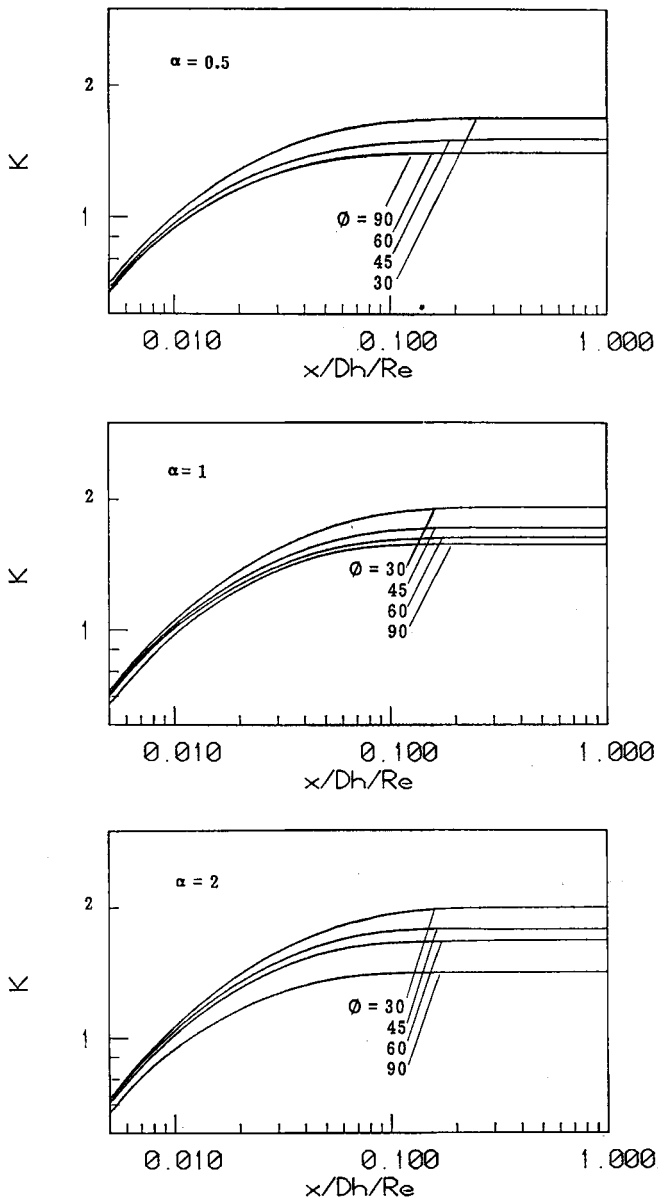

Figure 5. Incremental pressure drop K versus $x/(D_h/Re)$

cross-stream velocities become smaller as the fully developed region is approached. Comparison of velocity vectors for different ϕ and aspect ratios are presented in Figures 7 and 8 respectively. Figure 7 shows that the cross-stream velocity vectors of the trapezoidal duct with $\phi = 30°$ are stronger than for the others and the strength of the velocity reduces as ϕ increases. The figures show that the secondary flow is sucked towards the centre of the ducts. This can be explained as follows. The velocity gradient in the flow direction (centre part) is positive before reaching the fully developed region. In order to satisfy the continuity equation, the sum of the cross-stream

Table II. Fully developed values

ϕ (deg)	U_{max}/U_m		$(fRe)_{fd}$		$K(\infty)$			$K_d(\infty)$		$K_e(\infty)$	
	Present work	Shah and London[5]	Present work	Shah and London[5]	Present work*	Present work†	Shah and London[5]	Present work	Shah and London[5]	Present work	Shah and London[5]
					(a) $\alpha=0.5$						
90	1·984	1·992	15·488	15·548	1·410	1·354	1·383	1·337	1·347	2·014	2·039
60	1·965	1·969	15·351	15·693	1·412	1·334	1·379	1·335	1·349	2·002	2·039
45	2·001	1·998	15·052	15·206	1·513	1·400	1·464	1·347	1·367	2·047	2·099
50	2·091	2·073	14·348	14·323	1·686	1·550	1·651	1·375	1·404	2·150	2·229
					(b) $\alpha=1$						
90	2·081	2·096	14·181	14·227	1·575	1·516	1·552	1·368	1·378	2·126	2·154
60	2·099	2·119	13·883	14·151	1·637	1·596	1·618	1·388	1·392	2·186	2·201
45	2·141	2·169	13·594	13·827	1·721	1·700	1·744	1·407	1·418	2·257	2·290
30	2·232	2·266	13·045	13·246	1·916	1·930	1·969	1·456	1·457	2·431	2·442
					(c) $\alpha=2$						
90	1·984	1·992	15·488	15·548	1·410	1·354	1·383	1·337	1·347	2·014	2·039
60	2·138	2·162	13·597	13·804	1·674	1·610	1·687	1·386	1·404	2·191	2·248
45	2·193	2·232	13·234	13·364	1·776	1·710	1·847	1·403	1·434	2·258	2·358
30	2·290	2·352	12·770	12·875	1·992	1·876	2·115	1·431	1·482	2·369	2·540

* Figure 5.
† Equation (11).

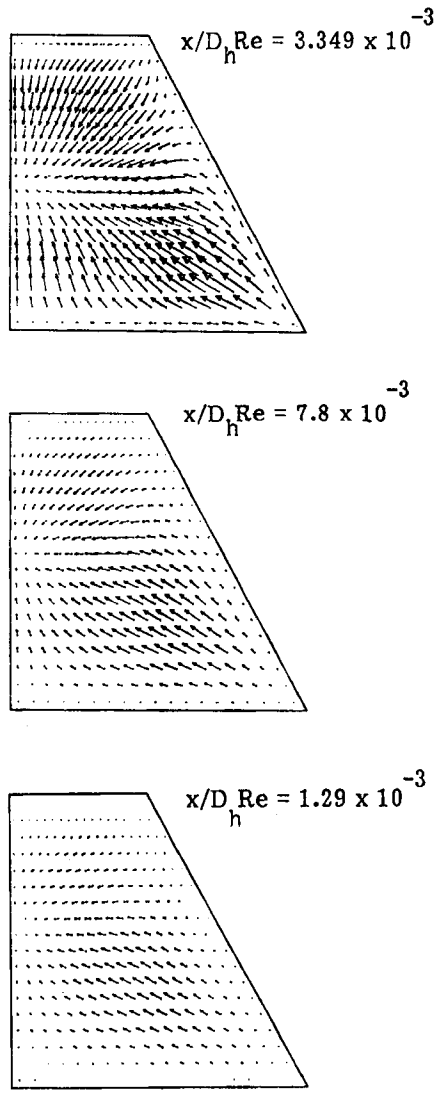

Figure 6. Velocity vectors at three axial positions ($\phi = 60°$; $\alpha = 1$)

gradients must become negative and fill the 'vacuum' occurring due to the increase in the main stream velocity.

The contours of the axial velocity at $x/(D_h Re) = 5{\cdot}57 \times 10^{-2}$ are plotted in Figure 9. As seen from this figure, the axial velocity at the centre part of the cross-plane increases with increasing aspect ratio α.

Momentum rate and kinetic energy. The variations of the momentum rate and kinetic energy along the axial length in the main flow direction are plotted in Figure 10. MoR and KE are greater than unity and 0·5 respectively for any non-uniform velocity distribution across the

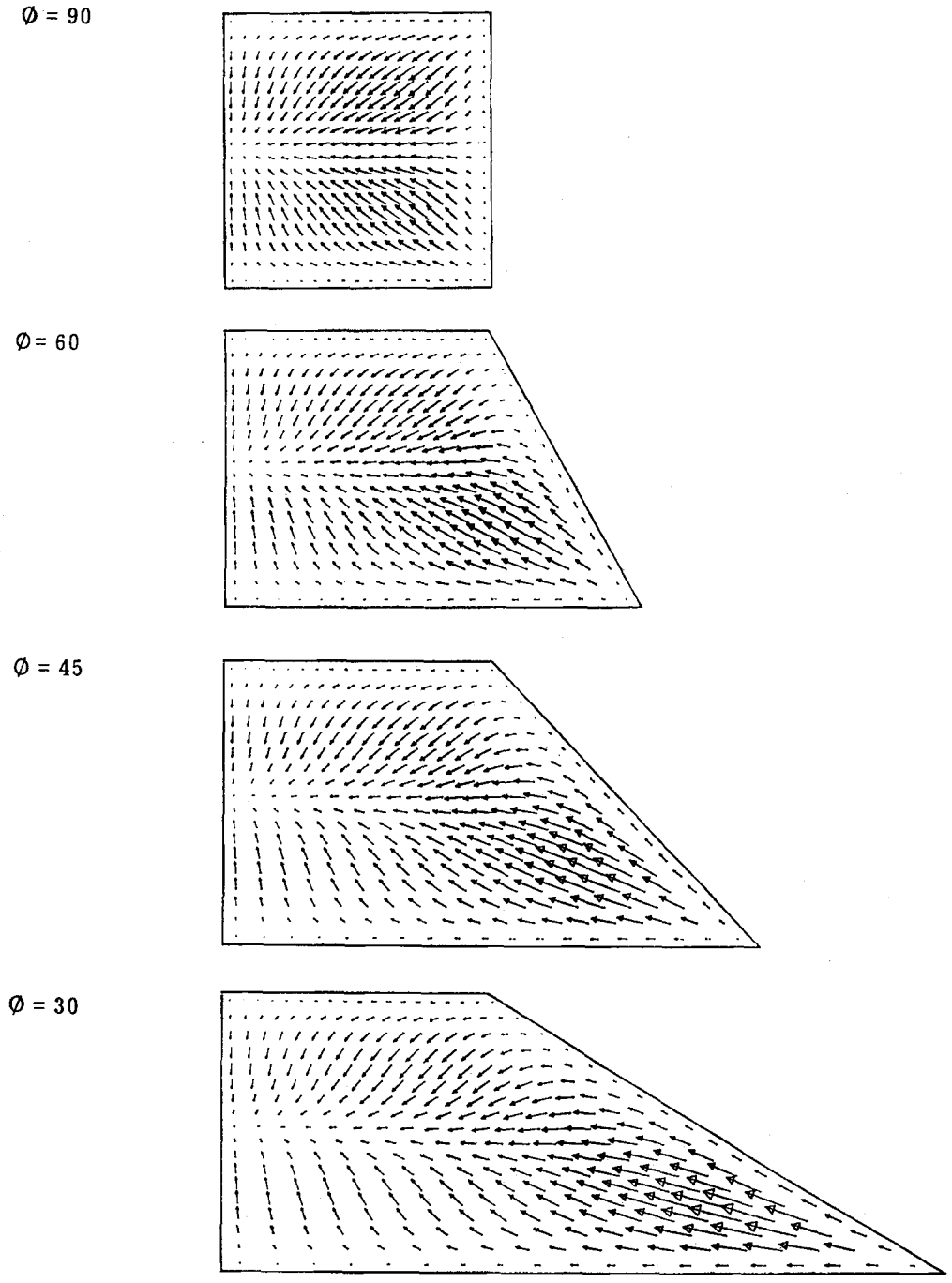

Figure 7. Velocity vectors for various ϕ-values ($\alpha = 0{\cdot}5$, $x/(D_h/Re) = 4{\cdot}64 \times 10^{-3}$)

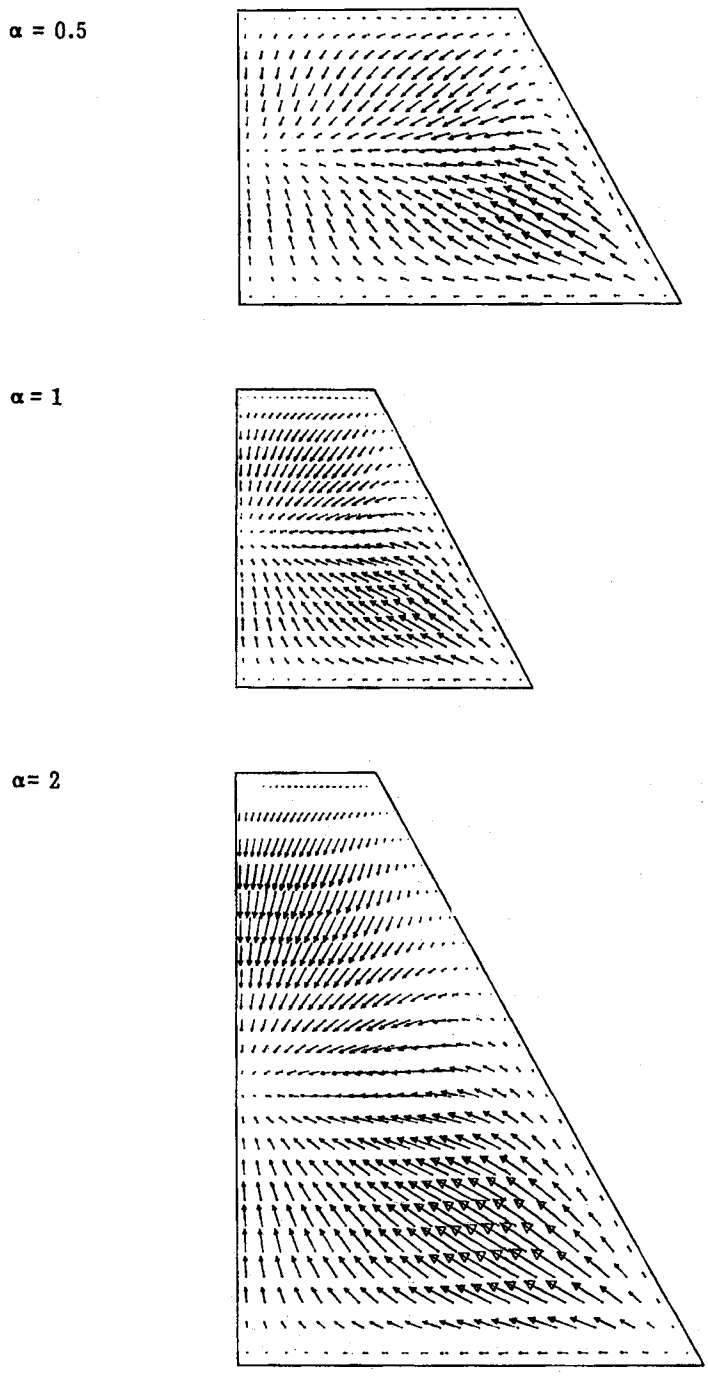

Figure 8. Velocity vectors for various aspect ratios ($\phi = 60°$, $x/(D_h/Re) = 4{\cdot}64 \times 10^{-3}$)

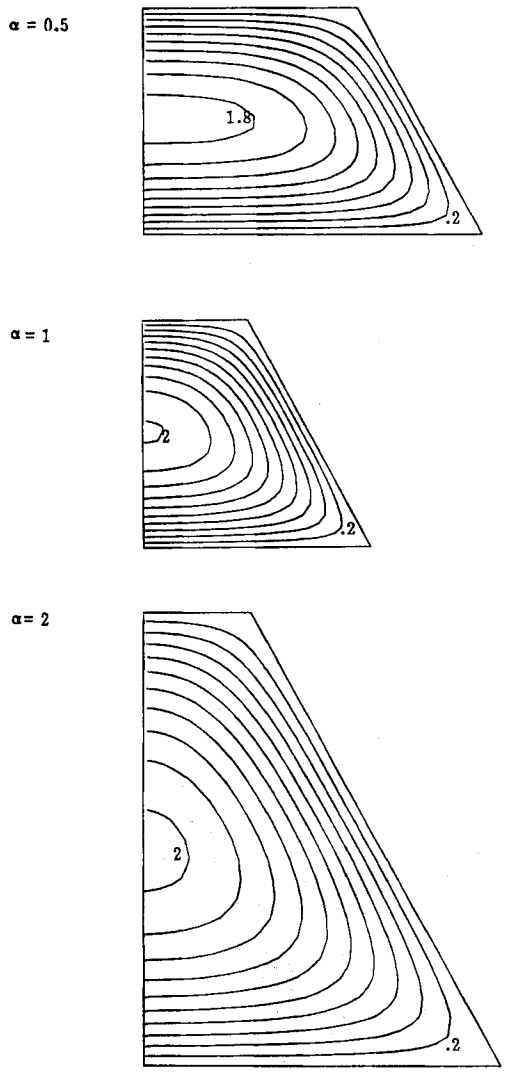

Figure 9. Axial velocity contours ($\phi = 60°$, $x/(D_h/Re) = 5{\cdot}57 \times 10^{-2}$)

section. In the entrance region the values of MoR and KE increase for a uniform entrance velocity profile and approach an asymptotic constant value at large axial distances.

The hydrodynamical results of the present work are compared with Shah[4] and listed in Table I. As seen from this table, the results of the present computation are in reasonable agreement with the values of Shah.

Thermal results

Comparison with the previous results. The comparison of the fully developed *Nu*-values for $\phi = 90°$ with available analytical and numerical results in the open literature is listed in

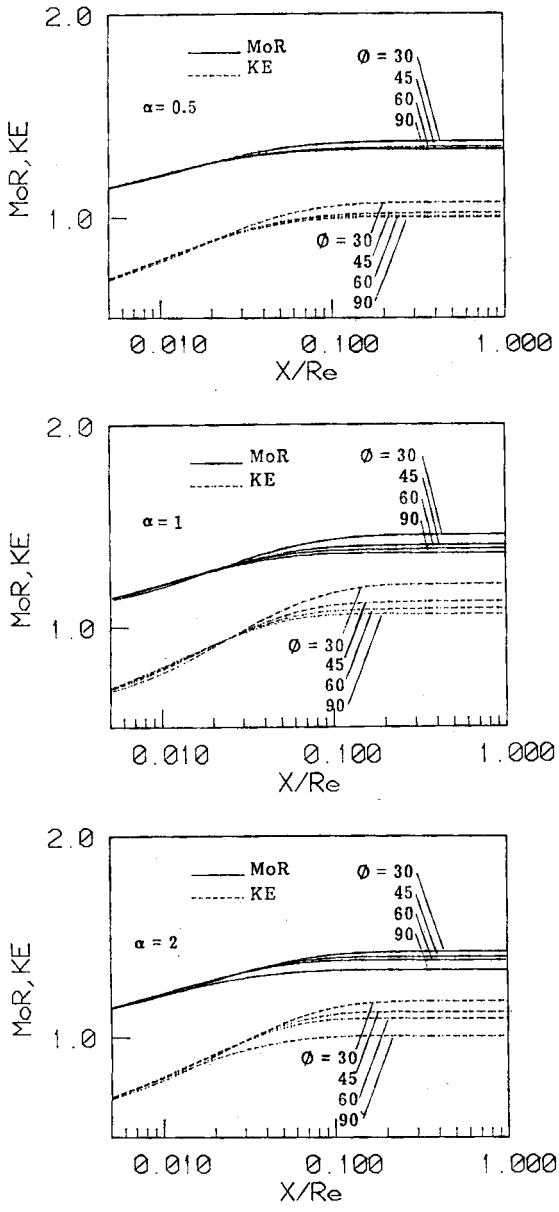

Figure 10. Momentum rate and kinetic energy variation in the main flow direction

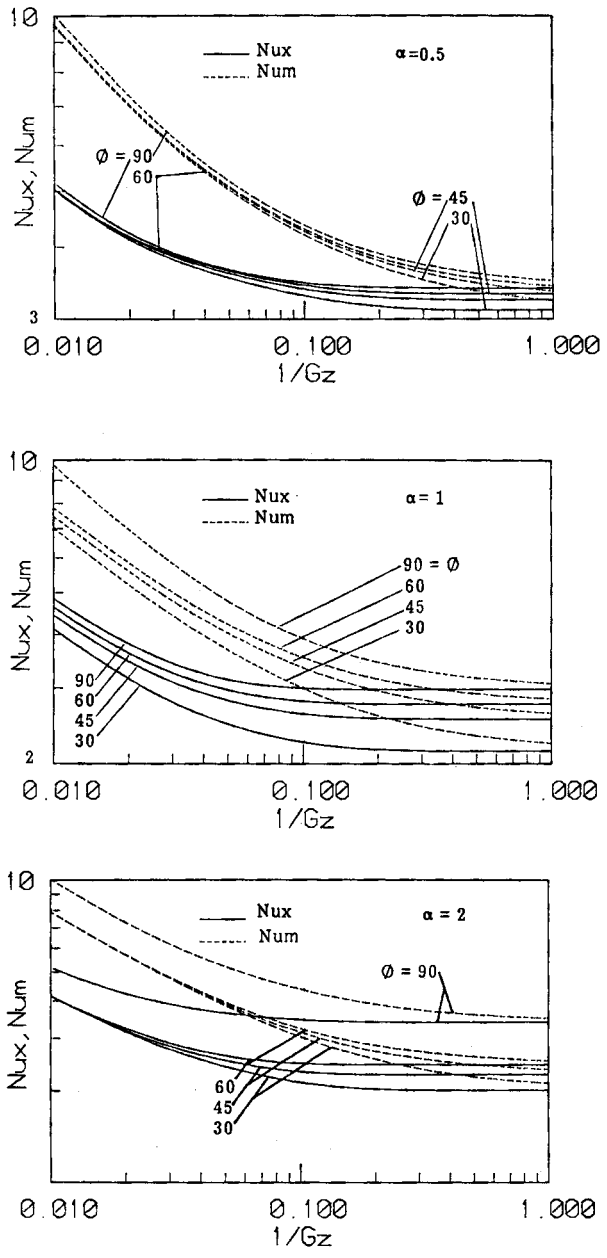

Figure 11. Local average Nusselt number Nu_x and average Nusselt number Nu_m versus reciprocal of Graetz number Gz

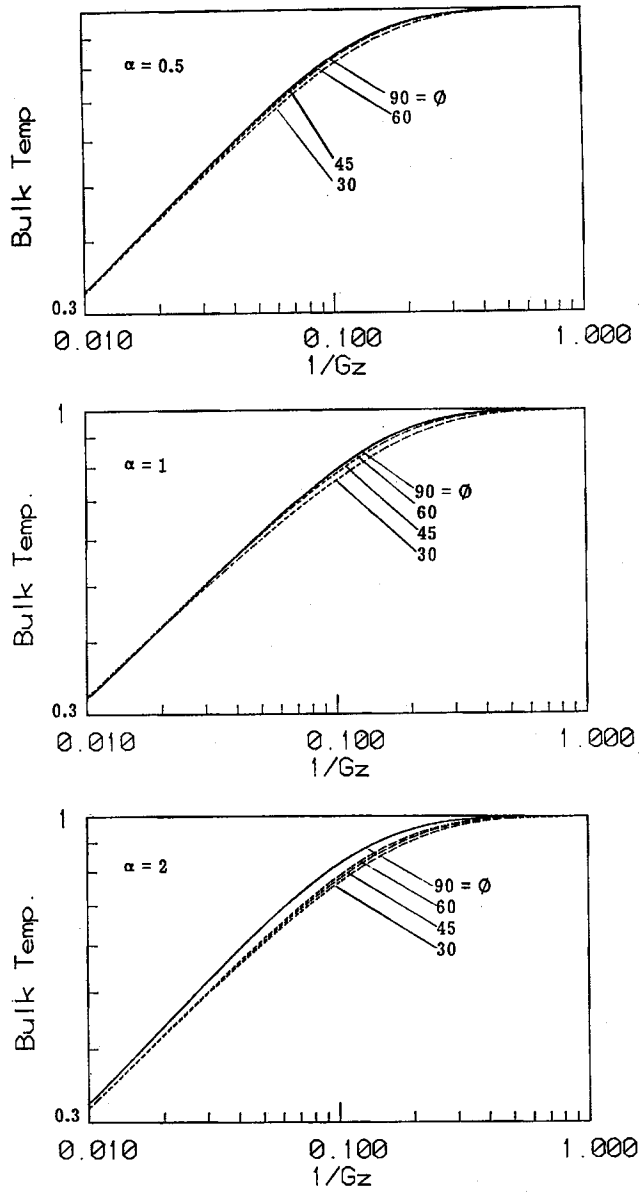

Figure 12. Bulk temperature variation versus reciprocal of Graetz number Gz for various aspect ratios

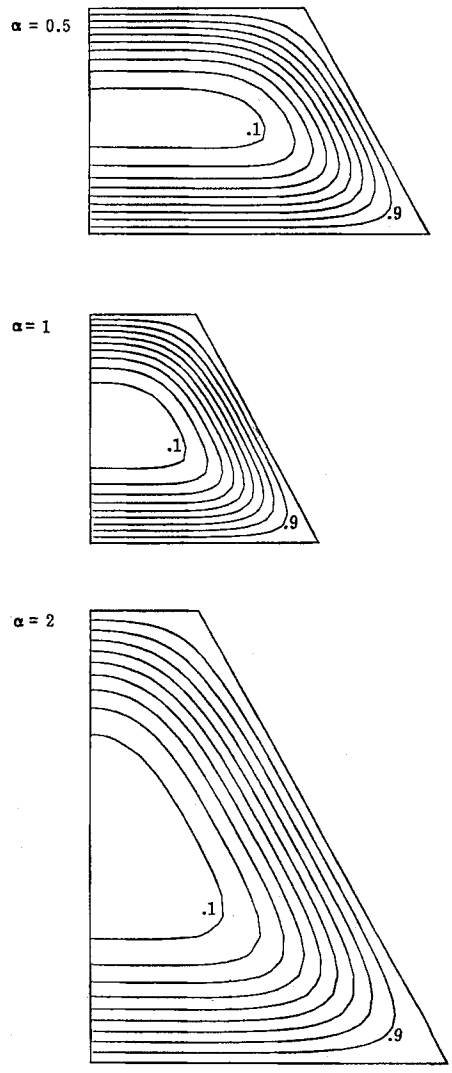

Figure 13. Isotherms at $x/(D_h/Re)=1{\cdot}085\times10^{-2}$ for various aspect ratios ($\phi = 60°$)

Table III. Comparison of the fully developed Nusselt number; computational and analytical results ($\phi = 90°$)

α	Present work	Aparecido and Cotta[25]	Asako *et al.*[12]	Shah and London[5]
1	2·981	2·978	2·980	2·976
2	3·393	3·392	—	3·391

Table III. The results of the present computations are in excellent agreement with the analytical results of Shah[4] and of Aparecido and Cotta[25] and with the numerical results of Asako *et al.*[12]

Nusselt numbers. Results for Nu_x and Nu_m for different aspect ratios are plotted in Figure 11 with ϕ as the curve parameter. As expected, Nu_x and Nu_m decrease with x and approach the fully developed values at large axial distances. As seen from the figures, Nu increases with increasing ϕ but increases as the aspect ratio is decreased.

Bulk temperature. The bulk temperatures for different aspect ratios are plotted in Figure 12 with ϕ as the curve parameter. These curves are consistent with the results obtained for the Nusselt numbers.

The isotherms at $x/(D_h Re) = 1{\cdot}085 \times 10^{-2}$ are presented in Figure 13.

CONCLUSIONS

A finite volume numerical method in complex three-dimensional geometries using co-located variables and Cartesian velocity components was employed to numerically investigate the characteristics of the simultaneously developing laminar flow and convective heat transfer in the entrance region of a trapezoidal duct under axially constant wall temperature. The influence of various geometrical dimensions of the cross-section on heat transfer and fluid flow were studied. The fully developed values of the Nusselt numbers, friction factors, axial velocity, incremental pressure drops and momentum rate and kinetic energy correction factors are close to the available asymptotic results. Increasing the aspect ratio of the trapezoidal duct reduces the heat transfer and increases the incremental pressure drop. Increasing the duct angle ϕ increases the heat transfer and decreases the incremental pressure drop.

ACKNOWLEDGEMENT

The present work is financially supported by the National Swedish Board for Technical Development (STU).

APPENDIX: NOMENCLATURE

A	area
a	coefficient in the discretized equations
C_p	specific heat
D_h	hydraulic diameter
$\mathbf{e}_i$	Cartesian unit base vector
f	friction factor

F	expansion factor
f_x	weighting factor
Gz	Graetz number ($=RePrD_h/x$)
$\mathbf{g}_i$	covariant base vector
g^{ij}	contravariant components of metric tensor
h	heat transfer coefficient
I	convective and diffusive fluxes
K	incremental pressure drop
K_d	momentum flux correction factor
K_e	kinetic energy correction factor
KE	kinetic energy
k	thermal conductivity
L	length of the duct
$\dot{m}$	mass flow rate
MoR	momentum rate
$\mathbf{n}$	normal vector
N	number of control volumes in a cross-section
Nu	Nusselt number ($=hD_h/k$)
p	pressure
Pr	Prandtl number ($=\mu c_p/k$)
Re	Reynolds number ($=u_{in}D_h/v$, u_mD_h/v)
S	source term
T	temperature
T_b	bulk temperature
U_i	dimensionless velocity
u, v, w	Cartesian velocity components
u_{in}	uniform inlet velocity
u_m	mean velocity

Greek symbols

α	aspect ratio (=height/top)
Γ	exchange coefficient
Δ, δ	prefixes denoting a difference
Θ	dimensionless fluid temperature for axially constant wall temperature
μ	dynamic viscosity
ν	kinematic viscosity
ξ_i	co-ordinate tangent to the grid lines
ρ	density
ϕ	angle of trapezoidal duct
Ψ	arbitrary dependent variable

Subscripts

NB	general neighbour grid point
E, P, W	refer to the grid nodes
e, w, s	refer to the control volume faces
n, l, h	refer to the control volume faces
fd	refers to the fully developed conditions

REFERENCES

1. S. V. Patankar and D. B. Spalding, 'A calculation procedure for heat, mass and momentum transfer in three-dimensional parabolic flows', *Int. J. Heat Mass Transfer*, **15**, 1787–1805 (1972).
2. C. Prakash and Ye-Di Liu, 'Analysis of laminar flow and heat transfer in the entrance region of an internally finned circular duct', *J. Heat Transfer*, **107**, 84–91 (1985).
3. K. C. Karki and S. V. Patankar, 'Heat transfer augmentation due to buoyancy effects in the entrance region of a shrouded fin array', *Proc. 23rd Natl. Heat Transfer Conf.*, Denver, CO, *ASME HTD Vol. 43*, 1985.
4. R. K. Shah, 'Laminar flow friction and forced convection heat transfer in ducts of arbitrary geometry', *Int. J. Heat Mass Transfer*, **18**, 849–862 (1975).
5. R. K. Shah and A. L. London, *Laminar Flow Forced Convection in Ducts*, Academic Press, New York, 1978.
6. B. R. Baliga and R. R. Azrak, 'Laminar fully developed flow and heat transfer in triangular plate-fin ducts', *J. Heat Transfer*, **108**, 24–32 (1986).
7. W. M. Kays and A. L. London, *Compact Heat Exchangers*, 3rd edn, McGraw-Hill, New York, 1984.
8. F. W. Schmidt and M. E. Newell, 'Heat transfer in fully developed laminar flow through rectangular and isosceles triangular ducts', *Int. J. Heat Mass Transfer*, **10**, 1121–1123 (1967).
9. E. Sparrow and A. Haji-Sheikh, 'Laminar heat transfer and pressure drop in isosceles triangular, right triangular, and circular sector ducts', *J. Heat Transfer*, **87**, 416–427 (1965).
10. G. E. Schneider and B. L. LeDain, 'Fully developed laminar heat transfer in triangular passages', *J. Energy*, **5**, 15–21 (1981).
11. M. Faghri, E. M. Sparrow and A. T. Prata, 'Finite difference solutions of convection–diffusion problems in irregular domains using a non-orthogonal coordinate transformation', *Numer. Heat Transfer*, **7**, 183–209 (1984).
12. Y. Asako, H. Nakamura and M. Faghri, 'Developing laminar flow and heat transfer in the entrance region of regular polygonal ducts', *Int. J. Heat Mass Transfer*, **31**, 2590–2593 (1988).
13. Y. Asako and M. Faghri, 'Three-dimensional laminar heat transfer and fluid flow characteristics in the entrance region of a rhombic duct', *J. Heat Transfer*, **110**, 855–861 (1988).
14. H. Y. Zhang, M. A. Ebadian and A. Campo, 'Computation of heat and fluid flow in ducts of arbitrary cross section', *Numer. Heat Transfer, Part A*, **17**, 231–248 (1990).
15. C. M. Rhie and W. L. Chow, 'Numerical study of the turbulent flow past an airfoil with trailing edge separation', *AIAA J.*, **21**, 1527–1532 (1983).
16. A. D. Burns and N. S. Wilkes, 'A finite difference method for the computation of fluid flow in complex three-dimensional geometries', *AERE R 12342*, Harwell Laboratory, 1986.
17. S. Majumdar, 'Developing of a finite volume procedure for prediction of fluid flow problems with complex irregular boundaries', *SFB 210/T/29*, University of Karlsruhe, 1986.
18. M. Peric, R. Kessler and G. Scheuerer, 'Comparison of finite-volume numerical methods with staggered and colocated grids', *Comput. Fluids*, **16**, 389–403 (1988).
19. T. F. Miller and F. W. Schmidt, 'Use of a pressure-weighted interpolation method for the solution of the incompressible Navier–Stokes equations on a non-staggered grid system', *Numer. Heat Transfer*, **14**, 213–233 (1988).
20. S. Majumdar, 'Role of underrelaxation in momentum interpolation for calculation of flow with non-staggered grids', *Numer. Heat Transfer*, **13**, 125–132 (1988).
21. F. Irgens, 'Tensoranalyse og kontinumsmekanikk, del III', Institutt for Mekanikk, Norge Tekniska Hoskole, Trondheim, 1966 (in Norwegian).
22. S. V. Patankar, *Numerical Heat Transfer and Fluid Flow*, McGraw-Hill, Washington, 1980.
23. L. Davidson, 'CALC-BFC: a finite-volume code for complex three-dimensional geometries using colocated variables and Cartesian velocity components', unpublished report, Chalmers University of Technology, Department of Applied Thermodynamics and Fluid Mechanics, 1989.
24. G. S. Beavers, E. M. Sparrow and R. A. Magnuson, 'Experiments on hydrodynamically developing flow in rectangular ducts of arbitrary aspect ratio', *Int. J. Heat Mass Transfer*, **13**, 689–702 (1970).
25. J. B. Aparecido and R. M. Cotta, 'Thermally developing laminar flow inside rectangular ducts', *Int. J. Heat Mass Transfer*, **33**, 341–347 (1990).